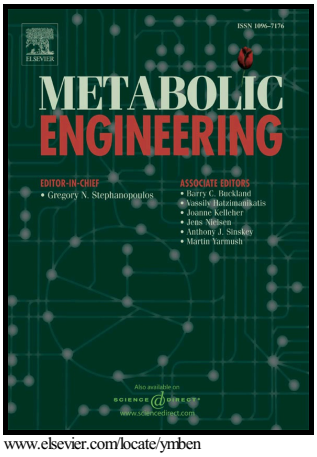

www.elsevier.com/locate/ymben

Design, development and application of whole-cell based antibiotic-specific biosensor

Yuriy Rebets, Stefan Schmelz, Oleksandr Gromyko, Stepan Tistechok, Lutz Petzke, Andrea Scrima, Andriy Luzhetskyy

PII: S1096-7176(18)30010-7
DOI: https://doi.org/10.1016/j.ymben.2018.03.019
Reference: YMBEN1374

To appear in: *Metabolic Engineering*

Received date: 12 January 2018
Revised date: 16 March 2018
Accepted date: 29 March 2018

Cite this article as: Yuriy Rebets, Stefan Schmelz, Oleksandr Gromyko, Stepan Tistechok, Lutz Petzke, Andrea Scrima and Andriy Luzhetskyy, Design, development and application of whole-cell based antibiotic-specific biosensor, *Metabolic Engineering,* https://doi.org/10.1016/j.ymben.2018.03.019

Design, development and application of whole-cell based antibiotic-specific biosensor

Yuriy Rebets[a,b1], Stefan Schmelz[c,1], Oleksandr Gromyko[d], Stepan Tistechok[d], Lutz Petzke[e], Andrea Scrima[c]*, Andriy Luzhetskyy[a,b]*

[a]Universität des Saarlandes, Pharmazeutische Biotechnologie, Bld. C2.3, 66123 Saarbrücken, Germany.

[b]Helmholtz-Institute for Pharmaceutical Research Saarland, UdS Campus, Bld. E8.1, 66123 Saarbrücken, Germany.

[c]Helmholtz-Centre for Infection Research, Inhoffenstrasse 7, 38124 Braunschweig, Germany.

[d]Ivan Franko National University of Lviv, Department of Genetics and Biotechnology, Hrushevskogo Street 4, 79005 Lviv, Ukraine

[e]BASF SE, 67056 Ludwigshafen, Germany

*Corresponding authors: Andrea.Scrima@helmholtz-hzi.de (Andrea Scrima), a.luzhetskyy@mx.uni-saarland.de (Andriy Luzhetskyy).

Abstract

Synthetic biology techniques hold great promise for optimising the production of natural products by microorganisms. However, evaluating the phenotype of a modified bacterium represents a major bottleneck to the engineering cycle – particularly for antibiotic-producing actinobacteria strains, which grow slowly and are challenging to genetically manipulate. Here,

[1] These authors equally contributed to this work

we report the generation and application of antibiotic-specific whole-cell biosensor derived from TetR transcriptional repressor for use in identifying and optimising antibiotic producers. The constructed biosensor was successfully used to improve production of polyketide antibiotic pamamycin. However, an initial biosensor based on native genetic elements had inadequate dynamic and operating ranges. To overcome these limitations, we fine-tuned biosensor performance through alterations of the promoter and operator of output module and the ligand affinity of transcription factor module, which enabled us to deduce recommendations for building and application of actinobacterial biosensors.

Keywords: whole cell biosensor, actinobacteria, secondary metabolite, antibiotic, polyketide, TetR repressor protein.

Abbreviations:

TFR, transcription factor of the TetR family; EMSA, electrophoretic mobility shift assay; LBD, ligand-binding domain; DBD, DNA-binding domain.

1. Introduction

Natural products of bacterial origin have an outstanding track record as sources of bioactive compounds (with, for example, anti-cancer or antibiotic activity), and they remain the major source of drug leads (Berdy, 2012; Newman and Cragg, 2016). However, many natural products with useful bioactivities are abandoned at a very early stage of drug development because of

low production levels and unavailable or inefficient chemical syntheses. To increase the yield of a natural product to enable the development of a particular compound as a useful drug, the producing strain has to be optimized.

Conventional and synthetic biology approaches provide a great selection of methods to increase genetic diversity in order to increase the production of natural products (Bilyk et al., 2013; Isaacs et al., 2011; Zhang et al., 2017). However, the identification of the improved strain among hundreds of thousands of mutants remains an unresolved challenge, as currently no method for the direct selection of strains with a high level of production of a natural product is available.

One potential approach for solving this problem is the direct detection and quantification of a metabolite of interest by utilization of a compound-specific whole-cell biosensor delivering a particular phenotype as specific readout. Such biosensor is typically composed of three modules: (i) the signal input module, based on a ligand-regulated transcription factor; (ii) the regulatory module, consisting of a signal input module-dependent promoter; and (iii) the signal output module, commonly a reporter or antibiotic resistance gene that allows for the detection, recording and quantification of the signal (**Fig. 1a**) (De Paepe et al., 2017; Rogers et al., 2016). The key characteristics of any sensor are specificity and sensitivity as well as operating and dynamic ranges (**Fig. 1b**). However, only a small proportion of the large number of bacterial transcription factors identified have been characterized in terms of their ligand specificity, and therefore only few could be used to build metabolite-specific biosensors (Dietrich et al., 2013; Raman et al., 2014; Rogers and Church, 2016a; Tang and Cirino, 2011). Moreover, we just began to gain a deeper understanding of basic design rules for the

development of biosensors with the desired properties (Mannan et al., 2017). Critically, most of the advances in biosensors application to date relate to molecules generated by primary metabolism, rather than the more structurally complex natural products.

Here, we report the design, development and application of a whole-cell biosensor for the detection and quantification of the macrodiolide antibiotic pamamycin produced by *Streptomyces alboniger* DSM-40043 (**Fig. 2a**). We chose a *Streptomyces* species because these bacteria are prolific producers of natural products and the methodology should therefore be applicable to a great number of compounds. The work presented here also led to the discovery of several principles for guiding the design of antibiotic-specific biosensors. These principles can be directly applied to strain improvement and will facilitate the search for new producers of a desired metabolite.

2. Materials and methods

2.1. Bacterial strains and culturing conditions

S. alboniger DSM-40043 is natural producer of pamamycins and puromycin (Porter et al., 1952) and was obtained from Leibniz Institutes DSMZ-German Collection of Microorganisms and Cell Cultures. *S. alboniger* Δ0734 is a non-producing derivative of DSM 40043 with a deletion of the *pamD* gene (Rebets et al., 2015b). *S. albus* J1074 (Chater and Wilde, 1980) and *S. albus* Δ*pseB4* (Bilyk and Luzhetskyy, 2014b) with only one øC31 actinophage *attB* site were used as hosts to evaluate the designed biosensor constructs and *pam*-gene cluster cosmid R2 expression. All *Streptomyces* plasmids are based on pTES (Herrmann et al., 2012) or pUWLH (Fedoryshyn et al., 2008) vectors. The plasmids pGUS-MF-PPV(a) and pGUS-MF-PPV(c),

encoding *gusA*^{ATG} and *gusA*^{CTG} alleles of the reporter gene, respectively, were used to generate transcription fusion and biosensor constructs (Ahmed et al., 2017). *Escherichia coli* XL1 Blue (Stratagene) was used for routine cloning applications. Proteins were purified from *E. coli* BL21(DE3) (Studier and Moffatt, 1986) carrying plasmids based on the vectors pET28b (for PamR2) (Novagen). *E. coli* ET12567 (pUB307) was used as a donor of plasmids in intergeneric conjugations (Flett et al., 1997). *E. coli* strains were grown in LB medium. *Streptomyces* spp. strains were grown on mannitol soy flour agar (MS agar) (Kieser T., 2000) and in liquid TSB medium (Sigma-Aldrich, USA). UV and chemical mutagenesis were performed by standard procedures, except that mycelia were used instead of spores (Kieser T., 2000). Production of pamamycins was assayed in SGG medium (Rebets et al., 2015b). The following antibiotics were used when required: apramycin (50 μg/ml), kanamycin (30 μg/ml and higher), spectinomycin (50 μg/ml) and phosphomycin (100 μg/ml) (Sigma-Aldrich, USA).

2.2. Isolation and manipulation of DNA

DNA extraction and manipulation, *E. coli* transformation and *E. coli*/*Streptomyces* spp. intergeneric conjugation were performed according to standard protocols (Kieser T., 2000; Rebets et al., 2017). Plasmids were constructed by conventional DNA ligation using T4 DNA ligase. DNA fragments were amplified with Phusion High-Fidelity DNA polymerases (Thermo Fisher Scientific, USA). All plasmids were verified by sequencing (GATC Biotech, Germany). Primers used in this work are listed in Table S1 and were supplied by Eurofins Genomics (Germany). Enzymes were used according to the manufacturers' recommendations (Thermo Fisher Scientific, USA; New England Biolabs, USA).

2.3. Plasmid construction

The *pamA* promoter was amplified by PCR using *S. alboniger* chromosomal DNA as template and cloned as *Kpn*I-*Bam*HI fragment into linearized pGUS-MF-PPV(a) vector. *pamR2* and the *pamW* promoter region were amplified with the use of the 0727PFXbI/0726REcV primer pair and cloned into pGUS-MF-PPV(a) as an *Xba*I-*Eco*RV fragment to generate the G0 biosensor construct. The *neo* gene was amplified from plasmid pIJ487 (Kieser T., 2000) and cloned into the pGUS-MF-PPV(a)-based G0 biosensor construct using *Kpn*I-*Not*I, thereby replacing the *gusA* reporter gene. The G1 pamamycin biosensor plasmid were produced by amplifying *pamR2* with the 0726REcV reverse primer in combination with a forward primer carrying the synthetic promoter of choice (Siegl et al., 2013a), PamR2 operators and the priming site, complementary to the promoter region of *pamR2* gene. For protein purification, the *pamR2* coding region was amplified by PCR using *S. alboniger* chromosomal DNA as template and cloned using *Nco*I-*Xho*I into pET28b; the *chdA* coding region was amplified from the chromosome of *A. sulphurea* and cloned by *Nco*I-*Eco*RI into pEHISTEV (Liu and Naismith, 2009). The point mutations in *pamR2* gene were introduced using the QuikChange II Site-Directed Mutagenesis kit (Agilent Technologies, USA). The G2 biosensors were constructed using a two-step overlapping PCR approach with a combination of R2D10O1FXbI and 0726REcV external primers and internal primers carrying the specific mutation. All sequences were verified by sequencing and visualized and analysed using Geneious, version 8.1.7 (Biomatters Ltd, New Zealand).

2.4. RNA sequencing

Whole-transcriptome shotgun sequencing was performed by Vertis Biotechnologie AG (Germany). Samples of *S. albus* J1074 carrying the R2 cosmid with the entire *pam* gene cluster grown in TSB media were collected after 36 hours, and total RNA was isolated using the peqGOLD TriFast reagent (PEQLAB, Germany) including DNase treatment; rRNA was depleted with the Ribo-Zero Bacteria kit (Epicentre, USA); and total RNA was used to synthesize cDNA. The sequencing was performed using the HiSeq 2000 platform (Illumina, USA), resulting in the production of 443.3 Mbp of 100 bp-long sequences. Sequences were end-trimmed using Geneious, version 8.1.7 (Biomatters Ltd, New Zealand), and mapped to the *S. albus* J1074 genome with the R2 cosmid sequence inserted into the øC31 actinophage *attB* site position with the Prokars Prokaryotic RNA-Seq analysis tool (http://prokars.org/, Dr. B. Tokovenko, personal communication). The complete set of RNAseq data is provided in Table S2.

2.5. Characterization of biosensors

β-glucuronidase activity was assayed *in vivo* and *in vitro.* For the *in vivo* test, spores of the biosensor strain were plated on MS agar supplemented with 50 µg/ml X-Gluc (X-Gluc Direct, Spain), and discs containing different compounds of interest were applied. Plates were visually monitored every 12 hours for the development of blue halos around discs. To quantify reporter activity, strains were grown in 10 ml of TSB at 28° C and 200 rpm for 1 day, and 0.5 ml of pre-culture was inoculated into 10 ml of fresh TSB. The inducer compound was added until the desired concentration was achieved after 12 h of growth, and flasks were subsequently incubated for another 12 hours. One millilitre of each culture was removed and β-

glucuronidase activity was measured and calculated as previously described (Siegl et al., 2013a). Experiments were performed in triplicate.

2.6. Pamamycin production analysis

Pamamycins were extracted as previously described (Rebets et al., 2015b). Metabolites were analysed on a Waters BEH C18 column (100 mm x 2.1 mm, 1.7 µm, column temperature 45 °C) using a UPLC-ESI-MS instrument (Dionex Ultimate 3000, Thermo Fisher Scientific and amaZon Speed ETD, Bruker). Samples were eluted with solvent A: ammonium formate buffer 90 mM and solvent B: 80:20 acetonitrile/100 mM ammonium formate buffer in a multistep gradient: 0.2 min 10 % B, 10 % B to 69 % B in 4 min, 69 % B to 87.5 % B in 26 min, 87.5 % B to 95 % B in 0.5 min, 1 min 95 % B, 100 % B to 10 % B in 0.5 min, 4 min equilibration at 10 % B. Reference samples of different concentrations of pamamycin 607 (1, 2.5, 5, 10 and 15 µg/ml) were used to build the calibration curve for production quantification. For extracts from new producer strains, samples were additionally analysed on a maXis 4G hr-ToF ultrahigh-resolution mass spectrometer using the Apollo II ESI source (Bruker Daltonics, Germany). Extracts were separated on UPLC system (Dionex Ultimate 3000, Thermo Fisher Scientific GmbH) with a Waters BEH C18 column (100 mm x 2.1 mm, 1.7 µm, column temperature 45 °C); 0.1 % formic acid was used as solvent A and 100 acetonitrile as solvent B. Samples were eluted with a gradient of solvent B from 5 to 95 % in 18 minutes. The flow rate was 0.5 ml/min.

2.7. Protein purification

PamR2 proteins were purified from *E. coli* BL21(DE3) strain carrying respective expression plasmids. The *E. coli* culture was grown in LB medium at 37 °C until an OD600 of 0.6 was reached, and expression was induced through the addition of IPTG to a final concentration of 0.5 mM. The culture was incubated at 20 °C overnight; cells were harvested by centrifugation and lysed in lysis buffer (1x PBS, supplemented with 1 mM phenylmethylsulphonylfluoride (PMSF), 5 mM $MgCl_2$, 80 µg DNase) using a homogenizer. DNA contamination was removed by ion exchange chromatography. The eluted protein fraction was diluted 1:3 with buffer A (50 mM Tris pH 8.0, 5 mM β-mercaptoethanol ((BME)) and loaded with 10 % buffer B (1 M NaCl, 50 mM Tris pH 8.0, 5 mM BME) on a SOURCE Q15 column (GE Healthcare). Protein was eluted with a gradient from 10 to 100 % buffer B over 20 column volumes. DNA-free protein was concentrated and further purified on a Superdex200 26/60 column. Protein was eluted in 50 mM Tris pH 8.0, 200 mM NaCl, and 5 mM BME, and pooled protein fractions were concentrated to 9 mg ml^{-1}. Aliquots were flash-frozen in liquid nitrogen and stored at -80 °C for further use.

2.8. Electrophoretic mobility shift assay (EMSA)

EMSA was performed in reaction buffer containing 20 mM TrisHCl pH 7.2, 120 mM NaCl, 2 mM $MgCl_2$ and 50 pM of double-stranded target DNA in a total volume of 20 µl at room temperature. Samples were resolved by native PAGE in 10 % gel, stained with ethidium bromide and visualized using a GelDoc station (Bio-Rad, USA). When testing the pamamycin affinity, the reaction mixture containing 1.7 µM of PamR2 protein and target DNA was pre-incubated at room temperature for 10 min, and aliquots of 18 µl were added to non-sticky 200

µl PCR tubes containing 2 µl of pamamycin solutions of different concentrations. DMSO was used as a negative control. Samples were mixed, incubated at RT for another 10 minutes and resolved by native PAGE in 10 % gel.

2.9. Crystallization of PamR2

Apo-PamR2 and PamR2 in complex with pamamycin 607 (P607) were crystallized by the sitting-drop vapour diffusion method. Apo-PamR2 was crystallized by mixing equal volumes of protein (4 mg ml^{-1}) and precipitant solution. Initial crystals grew within five days in A7 of the JCSG Core1 screen (0.2 M tri-Potassium citrate, 20 % (w/v) PEG 3350; Qiagen, USA) at 20 °C. Further optimization, using custom-made 96-well screens, resulted in larger crystals (110 × 130 × 80 µm) of the C2 space group. Crystals grew in 150 mM sodium chloride and 722 mM tri-lithium citrate with 5 mg ml^{-1} PamR2, reaching their full size within 2 weeks at 20 °C. Crystals were cryo-protected in 12 % (v/v) (*2R,3R)*-(-)-2,3-butanediol and flash-frozen in liquid nitrogen for data collection. PamR2 in complex with P607 was co-crystallized in 0.1 M CHES pH 8.8, 0.7 M tri-sodium citrate, and 0.14 M tri-lithium citrate with 5 mg ml^{-1} protein, which was pre-incubated with 0.5 mM P607 (dissolved in 1:1 DMSO:methanol) for 10 min on ice. Crystals (180 x 180 x 160 µm) with a hexagonal ($P6_222$) shape started to grow after more than 65 days at 20 °C. Crystals were cryo-protected in 30 % (v/v) glycerol and flash-frozen in liquid nitrogen for data collection.

2.10. X-ray data collection and structure determination

Data for apo-PamR2 were collected at beamline 14.2 at the Helmholtz-Zentrum Berlin BESSY II synchrotron at a wavelength of 0.918 Å at 100 K. Data were processed, scaled and merged using the XDS package (Kabsch, 2010). The initial MR model was identified using BALBES (Long et al., 2008), which determined the TetR-like repressor SimR to be the best model (PDB code: 2Y30) (Le et al., 2011). The final model was built manually using Coot (Emsley and Cowtan, 2004) with iterative refinement steps of phenix.refine (PHENIX package (Afonine et al., 2012)).

Data for the P607 co-complex were collected at beamline 14.2 at the Helmholtz-Zentrum Berlin BESSY II synchrotron at a wavelength of 0.918 Å at 100 K. The refined apo-PamR2 model was used as an MR model for the $P6_222$ crystals of the co-complex using Phaser-MR (Mccoy et al., 2007). The final co-complex model was finalized with Coot and phenix.refine. Restraints for the P607 ligand were generated with eLBOW .

Values in parentheses refer to the highest resolution shell. $R_{merge} = \frac{\sum_{hkl}\sum_j |I_{hkl,j} - \langle I_{hkl}\rangle|}{\sum_{hkl}\sum_j I_{hkl,j}}$ and $R_{meas} = \frac{\sum_{hkl}\sqrt{\frac{n}{n-1}}\sum_{j=1}^{n}|I_{hkl,j} - \langle I_{hkl}\rangle|}{\sum_{hkl}\sum_j I_{hkl,j}}$, where I is the measured intensity and <I> is the averaged intensity of each unique reflection with indices hkl. I/σ(I) corresponds to the average of the intensity divided by its average standard deviation. $R_{work/free} = \frac{\sum_{hkl}\left|F_{hkl}^{obs} - F_{hkl}^{calc}\right|}{\sum_{hkl} F_{hkl}^{obs}}$, where F_{obs} and F_{calc} are the observed and calculated structure factors, respectively. R_{free} is the same as R_{work}, calculated for the 5 % of the data that were randomly omitted from refinement. Protein structures were deposited in PDB: apo-PamR2 ID 5OJX and ligand-bound PamR2 ID 5OJY.

3. Results

3.1. Reporter-guided selection of pamamycin-overproducing strains

Pamamycins are a family of insecticidal and antimycobacterial macrodiolides produced by a polyketide assembly line (**Fig. 2a**) (Rebets et al., 2015a). Pamamycins provided an interesting and challenging test case for the design of secondary metabolite biosensors, for two reasons. Firstly, their lack of a chromophore prevents detection by liquid chromatography with photodiode array detection. Secondly, *S. alboniger* also synthesizes puromycin, a highly active nucleoside antibiotic, (Abou-Zeid and el-Dewany, 1973) which complicates the detection of pamamycins by antibacterial activity assays. Although a specific LC-MS detection and quantification method can be used, (Rebets et al., 2015a) this method is time-consuming.

We initially attempted a straightforward approach based on the assumption that the expression level of the pamamycin biosynthetic genes correlates with the final yield of pamamycins (Xiang et al., 2009). We fused the ATG start-codon variant of the *gusA* (*gusA*^{ATG}) reporter gene (Myronovskyi et al., 2011) that encodes β-glucuronidase with the *pamA* promoter, which controls several key polyketide synthase genes responsible for the synthesis of pamamycin. Hence, transcription of the reporter gene should mirror the transcription of the synthesis genes. (**Fig. S1a,b**). *S. alboniger* DSM-40043 carrying this fusion plasmid was mutagenized, and the resultant mutant library was visually screened for clones with increased β-glucuronidase activity, as detected by the intensity of the blue halo surrounding the colony. One hundred ninety-eight selected colonies were re-evaluated for reporter activity (**Fig. S1c**), and production of pamamycins by the eight most intensely coloured strains was assessed by

LC/MS. Only four of these strains showed an increase in pamamycins production, ranging from 3-fold to 4-fold. (**Fig. S1d**).

This false-positive rate (50 %) was similar to previous observations using this approach, and likely stems from the decoupling of transcription levels with final compound yields (Xiang et al., 2009). The low hit rate of this system (only 8 out of 196 pre-selected strains displayed the screening phenotype and advanced to the testing phase) made it necessary to develop a more refined approach.

3.2. Construction of a Generation 0 (G0) pamamycin biosensor

In contrast to reporter-guided selection, whole-cell biosensors provide the advantage that the metabolite is directly detected and its levels can be quantitated. The pamamycin biosynthetic cluster, like many secondary metabolite synthesis clusters in actinobacteria (Ostash et al., 2008; Tahlan et al., 2008), contains genes encoding a putative transporter (*pamW*) and a transcription factor in the TetR family (TFR, *pamR2*) (**Fig. S1a**) that together facilitate the export of pamamycin in response to its intracellular concentration. We fused the *pamW* promoter to *gusA*^{ATG}, which connects transcription of the reporter gene with PamR2 control (**Figure 2b**), forming the G0 sensor. This approach should make the expression of *gusA* directly dependent on the concentration of pamamycin. As a proof of principle, we first introduced the biosensor into *Streptomyces albus* Δ*pseB4* (Bilyk and Luzhetskyy, 2014a); this strain does not produce pamamycins, and hence exposure of the resulting strain to pamamycin 607 should lead to *gusA* induction (**Fig. S2a-e**). The operating range of the G0 biosensor in *S. albus* Δ*pseB4* was determined to be 0.05 - 1 mg/L (**Fig. 2c,d, Fig. S2f**), whereas the operating

range was determined to be to 0.1 – 2.5 mg/L in the pamamycin-deficient *S. alboniger* Δ0734 (Rebets et al., 2015a), (**Fig. 2c,d**, **Fig. S2g**). Because this latter strain still produces the pamamycin exporter PamW, which lowers the intracellular pamamycins concentration, this shift was expected. When the biosensor was used in the pamamycin-producing strain *S. alboniger* DSM-40043, we obtained similar results: at the highest pamamycins production level (5-7 mg/L), the activity of β-glucuronidase reached 70-80% of the observed maximum in *S. alboniger* Δ0734 (**Fig. S3**).

The colorimetric output of the G0 biosensor nevertheless required visual inspection of thousands of colonies to identify overproducers. We therefore changed the readout from reporter to selector by replacing *gusA* with the kanamycin resistance gene (*neo*) (**Fig. 2e)** (Kieser T., 2000). This G0-*neo* biosensor provided resistance of up to 100 μg/mL kanamycin when tested in *S. alboniger* DSM-40043. After UV-induced mutagenesis, we selected four colonies that were resistant to 200 μg/mL kanamycin and showed an increase in pamamycins production, ranging from 1.2-fold to 2.4-fold (15 - 16 mg/L) (**Fig. 2f; Table S3**). To estimate the correlation between biosensor activity and production level, we tested the survival of the highest- and lowest-producing mutants at different concentrations of kanamycin. The MIC values for the strains Neo21-4 and Neo18 were determined to be 300 and 700 μg/ml, respectively (data not shown). Both strains maintained resistance and production phenotypes after multiple passages through unselective conditions.

3.3. Functional characterization of transcription repressor PamR2

Despite the encouraging results obtained, the G0 system showed a high basal β-glucuronidase activity in the absence of pamamycin (**Fig. 2d**, **Fig. S2f,g**). To better understand the transcriptional organisation of the *pamR2 – pamW* intergenic region, we performed whole-transcriptome shotgun sequencing of the *S. albus* Δ*pseB4* strain carrying the entire pamamycin gene cluster. Crucially, we discovered that *pamW* is transcribed from two distinct promoters with respective transcription start sites located -64 and -44 bp (±5 bp) from the predicted start codon (**Fig. S4a**). We speculate that the promoter at -44 is a possible cause for the observed background noise of the G0 biosensor, as sequence analysis revealed that the *pamW* -64 promoter contains a palindromic repeat separated by one base pair (cTCGTACGaCGTACGA), and half of this repeat (CGTACGAgac) is located within the -44 promoter region (**Fig. S4a**). Data from electrophoretic mobility shift assay (EMSA) demonstrate that PamR2 efficiently binds to this repeat, which can be composed of either the entire -64 operator or half of the -64 operator and the -44 operator sequences placed in native or randomized surrounding sequence (**Fig. S4, S5**). This finding suggests that PamR2 might simultaneously repress both -64 and -44 promoters by bending the DNA region between them. The competing between binding sites apparently results in incomplete repression of the -44 promoter **(Fig. 2b)**.

3.4. Tuning pamamycin biosensor performance (Generation G1)

To improve the signal-to-noise ratio in the G0 biosensor, we constructed a G1 biosensor in which the two native *pamW* promoters were replaced with well-established synthetic promoters (the strong P21, the moderate B10 or the weak D10) (**Fig. 2f**) (Siegl et al., 2013b). The promoter was combined with one (O1) or two (O2) PamR2 operators located downstream

from the transcription start site, or with a single PamR2 operator sequence inserted between the -10 and -35 regions (Oi). These promoters were fused to *gusA*^{ATG}, and their response to pamamycin was tested in *S. albus* Δ*pseB4*. The G1 biosensors demonstrated greater dynamic range (**Fig. 2c,d**), but still showed high basal activity when tested *in vitro* and *in vivo* (**Fig. S6, S8**). We changed the *gusA* start codon to CTG (*gusA*^{CTG}) to decrease the translation initiation rate (Myronovskyi et al., 2011). This greatly improved the biosensor's properties; despite a lower absolute dynamic range, the relative dynamic range of these biosensors was improved because of the lower level of basal activity (**Fig. 2c,d, Fig. S7, S8**). The decrease in basal signal also caused a shift of operating range of the G1 sensors toward lower concentrations of pamamycin. The *gusA*^{CTG} biosensors behaved similarly in *S. alboniger* Δ0734 (**Fig. 2c,d, Fig. S9**). A comparison of the three operator position variants showed that O2 and Oi were not superior to the O1 design, demonstrating that the simplest architecture was most efficacious (**Fig. 2c-e)**.

3.5. Application of G1 biosensor

As further attempts to improve *S. alboniger* Neo18 by selection of clones with increased kanamycin resistance were not successful, we speculate that this strain has reached the limits of the biosensor system. We therefore took a different approach and analysed extracts of 750 Neo21-4 mutants for their ability to induce *gusA* expression in *S. albus* Δ*pseB4* carrying the G1 biosensor consisting of the *gusA*^{CTG}, the D10 promoter and the O1 operator (CD10RO1). Using this strategy, we were able to identify three strains (Neo21-4Rif1, Neo21-4Str6 and Neo21-4Str8) producing up to 30 mg/L of pamamycins **(Fig. 2f, Table S3)**.

The low noise and high sensitivity of the CD10RO1 construct further allowed us to screen 400 actinobacteria strains isolated from the rhizospheres of *Olea europaea* L. growing in the Nikita Botanical Gardens, Crimea, Ukraine, for new pamamycin producers. To simplify the procedure, the agar plaque diffusion test was used with *S. albus* Δ*pseB4* CD10RO1 as a test culture (**Fig. S10**). Eight strains were found to induce *gusA* expression in the reporter strain, seven of which produced pamamycins (**Fig. S11, S12**). However, the level of production was significantly lower than in *S. alboniger* DSM-40043. We obtained a further proof for pamamycin production by cloning and sequencing the *pamA* gene orthologues from the chromosomes of three of the newly identified pamamycin producers (Lv 20-116, Lv 20-124 and Lv 20-248), as well as from the strain Lv 50-79 for which pamamycin production was not confirmed by LC-MS (**Fig. S13**).

3.6. Development of G2 biosensors by reducing PamR2-pamamycin binding

The relatively low upper detection limit of the G1 biosensors remains the major drawback in their application for producing strain improvement. As we demonstrated above, with the *S. alboniger* Neo18 we reached the limits of the native PamR2-based biosensors performance. We hypothesized that the detection limit may be improved by reducing the affinity of PamR2 for pamamycins. To achieve the understanding of specificity and topology of PamR2 ligand binding, we determined the structures of PamR2 in the apo-form and bound to pamamycin 607 at resolution levels of 2.0 Å and 2.3 Å, respectively (**Fig. 3, Table S4**). This revealed that PamR2 forms a dimer reminiscent of other TFRs (Cuthbertson and Nodwell, 2013) and that the PamR2 monomer is composed of 12 α-helices, of which helices α1-α3 form the N-terminal DNA-binding

domain (DBD), mediating interaction with the operator and helices α4-α9 form the C-terminal ligand-binding domain (LBD), mediating dimerization and interaction with pamamycin. Dimerization is mainly facilitated by hydrophobic residues on α8 and α9, which contact the respective helices in the symmetry-related molecule. Apart from the canonical nine α-helices, PamR2 features three additional helices: an N-terminal α-helix (α0) connected to the DNA-binding domain (DBD) via a short flexible linker and two α-helices (αArm1, αArm2) inserted between α8 and α9, which form an 'arm' that extends from the LBD towards the LBD of the opposing protomer (**Fig. 3**).

Pamamycin binding induces a conformational change in the „arm-region", particularly in αArm1, resulting in a fully closed ligand binding pocket and compaction of the homodimer. The pamamycin-binding pocket is shaped by both monomers of PamR2, involving residues from α8, αArm1, αArm2 and α9 (and connecting loops) on one side, and residues from α6*, α7* and α8* (and connecting loops) on the other side, and provides two binding sites per dimer (**Fig. 3**). Except for the water mediated contact between the carbonyl-oxygen of pamamycin and the side-chain of S217, the PamR2 pamamycin 607 binding is mediated via a large number of hydrophobic interactions (**Fig. 3d,e, Fig. S14, S15**).

For the optimization of the biosensor, we designed mutations that would occlude the binding pocket, with the aim of reducing PamR2 pamamycin affinity. Ten individual mutant proteins, involving six different amino acids, were predicted to narrow the ligand selection by PamR2 (P129V, P129L, V131L, V168L, S173L, S173T, V214I, V214L, S217L, S217T) (**Fig. 3e,f**). The mutant proteins were purified and tested by EMSA to evaluate their DNA binding activity and affinity for pamamycin 607 and pamamycin 635 (**Fig. S16**). Two mutations, P129V and P129L,

caused a complete loss of the DNA binding activity of PamR2 (not shown). Five others (V131L, V168L, S173L, S173T, and V214I) demonstrated decreased affinity to pamamycin 635, of which the latter three also showed a slight decrease in pamamycin 607 binding affinity. V131L was combined with each of these latter three mutations, resulting in double mutants that demonstrated a further decrease in pamamycin 635 binding (**Fig. S17**). Finally, two triple mutant proteins were generated by adding the V168L or S173T mutation to the V131L/V214I double mutant **(Fig. 3f)**. Both triple mutant proteins showed significantly decreased pamamycin 635 binding as well as a decrease in affinity for pamamycin 607 (**Fig. S18**).

We generated two G2 biosensors based on the CD10O1 signal output module and mutants of PamR2 (V131L/V214I/V168L and V131L/V214I/S173T). Both G2 biosensors, when introduced into *S. albus* Δ*pseB4*, exhibited decreased sensitivity towards pamamycins 635 and 649 compared with the sensitivity observed for the respective G1 construct (**Fig. 4a**). While the V131L/V214I/V168L sensor retained a pamamycin 607 detection range similar to that of the G1 construct, the V131L/V214I/S173T mutant showed a more linear response to ligand concentrations with a clear shift in the upper limit of the operating range from 1 mg/L to more than 5 mg/L. When simulating natural conditions with an equimolar mixture of pure pamamycins or crude extract from the producing strain, the G2 biosensors demonstrated a strong improvement in the operating range over the G0 and G1 biosensors (**Fig. 4b,c**).

4. Discussion

The rapid development of synthetic biology tools in recent decades has resulted in significant progress in the metabolic engineering of microbes to produce specific chemicals

(Ajikumar et al., 2010; Brown et al., 2015; Paddon et al., 2013). Despite that, the evaluation of phenotypes in engineering cycles remains a major bottleneck (Dietrich et al., 2010; Rogers and Church, 2016b). Whole-cell biosensors provide the opportunity for multiplexing, thus accelerating the test step of the cycle (Dietrich et al., 2013; Raman et al., 2014; Rogers and Church, 2016a; Rogers et al., 2015). The majority of whole-cell biosensors are constructed from native components, which restricts their utility (Raman et al., 2014; Rogers et al., 2015). Additionally, current constructs are mainly devoted to compounds from primary metabolism and neglect more structurally complex secondary metabolites. Through our work aimed at improving the production of the antimycobacterial compound pamamycin in *S. alboniger*, we have developed the first design recommendations for the construction and tuning of biosensors to achieve better performance. We found that our G0 biosensors, consisting of a promoter (*pamW*) regulated by a native, pamamycin-responsive transcription factor, were poorly suited for downstream applications. We suggest that the limited operating and dynamic ranges of the sensor are due to the fact that the native receptor protein evolved to act over intracellular concentrations of ligand, rather than concentrations that are useful for applications of synthetic biology and biotechnology. This constraint was partially overcome by switching from selection (*Neo*) to screening (*gusA*) procedure, but this provided only a marginal increase in throughput of the procedure when compared to the conventional methods, like activity-based screening.

Manipulating the regulatory (promoter strength, operators number and location) and signal output modules (translation efficiency) of the sensor influenced the basal level of output signal and dynamic range, but had no major effect on the operating range. To optimize the regulatory module of a sensor, detailed knowledge of the functional properties of the regulatory protein

was required. Tuning the biosensor using promoters of different strengths led to lower basal signal and improved related dynamic range. The location of operator sequences had no significant effect, although care should be taken with placement of operators between -10 and -35, as this can affect overall promoter activity (Jensen and Hammer, 1998; Siegl et al., 2013b). Amplification of the output signal (by moderating the translation initiation rate through the alteration of the start codon of the reporter gene – *gusA*^{ATG} vs *gusA*^{CTG} in our case) should also be performed carefully, because of the high probability of increasing the system noise. From our experience it became obvious that the use of a strong promoter is preferred when tuning is aimed at increasing the dynamic range of the biosensor and a weak promoter when higher sensitivity is desired. A reporter with a high rate of translation initiation might be used as signal output module when a rapid response is aimed.

The operating range of a biosensor is a function of the intracellular concentrations of the receptor protein and ligand molecule and the affinity of the receptor for the operator DNA and ligand (Mannan et al., 2017). As the other repressed repressor proteins, PamR2 acts by an all-or-none principle (**Fig. S16**) (Novick and Weiner, 1957; Reichheld et al., 2009; Siegele and Hu, 1997). Thus, expansion of the operating range of transcriptional repressor based biosensors could be achieved in four ways: i) decreasing the effector concentration (for example, by active metabolite export by PamW, as observed in *S. alboniger* Δ0734); ii) increasing the expression level of the receptor protein (Wang et al., 2015); iii) increasing protein-DNA affinity (Mannan et al., 2017) or iii) decreasing the receptor's ligand affinity. The final approach is the preferred method, as it leads to higher orthogonality of the biosensor and can be tuned to achieve a greater shift in the operating range when combined with i) and ii). Changing the operator-

protein affinity, operators' number and locations while being potentially able to shift the operating range will also influence other parameters of the biosensor, including the basal output, dynamic and operating ranges and sensitivity. Tuning the receiver module could be achieved by both rational structure-driven and by random mutagenesis because the system allows for self-evaluation. We have employed the rational approach by mutating the PamR2 protein to narrow the selection of ligands and decrease the protein-ligand affinity, resulting in a shift of operating range from 1 mg/L in the case of G0 and G1 biosensors to more than 5 mg/L in the case of G2 biosensor, showing the feasibility of proposed strategy.

The development of biosensors for use in screening for antibiotic producers is more straightforward than the development of biosensors designed to screen for producers of other bacterial metabolites. The TetR family is the most abundant group of transcription factors in actinobacteria, (Cuthbertson and Nodwell, 2013; Romero-Rodriguez et al., 2015) and many members of that family are associated with the secondary metabolite biosynthetic gene clusters responsible for producing their ligands. At least 17 % of the secondary metabolite biosynthesis gene clusters of actinobacteria code for TetR-like genes coupled with the gene for putative transporter proteins, providing opportunities for the future development of antibiotic-specific biosensors. The design principles described here will aid in the development and tuning of these biosensors.

Acknowledgements

This work was supported by the DFG grant LU1524/4-1 and partially by the European Commission under the 7th Framework Program through the "Collaborative Project" action "STREPSYNTH" Grant no. 613877 to AL. X-ray data were collected at beamline 14.2 of BESSY II (Helmholtz-Zentrum Berlin (HZB), Berlin, Germany). We thank HZB for the allocation of synchrotron radiation beamtime and all the beamline staff for their support. Work in the group of A.S. is partially funded by the Helmholtz Association Young Investigator grant number VH-NG-727.

References

Abou-Zeid, A. Z., el-Dewany, A. I., 1973. Production and biosynthesis of puromycin by *Streptomyces alboniger*. Zentralbl. Bakteriol. Parasitenkd. Infektionskr. Hyg. 128**,** 635-59.

Afonine, P. V., et al., 2012. Towards automated crystallographic structure refinement with phenix.refine. Acta Crystallographica Section D-Biological Crystallography. 68**,** 352-367.

Ahmed, Y., et al., 2017. Identification of butenolide regulatory system controlling secondary metabolism in Streptomyces albus J1074. Sci Rep. 7**,** 9784.

Ajikumar, P. K., et al., 2010. Isoprenoid pathway optimization for taxol precursor overproduction in *Escherichia coli*. Science. 330**,** 70-74.

Berdy, J., 2012. Thoughts and facts about antibiotics: Where we are now and where we are heading. J. Antibiot. 65**,** 385-395.

Bilyk, B., Luzhetskyy, A., 2014a. Unusual site-specific DNA integration into the highly active pseudo-attB of the *Streptomyces albus* J1074 genome. Appl. Microbiol. Biotechnol. 98**,** 5095-5104.

Bilyk, B., Luzhetskyy, A., 2014b. Unusual site-specific DNA integration into the highly active pseudo-attB of the Streptomyces albus J1074 genome. Appl Microbiol Biotechnol. 98**,** 5095-104.

Bilyk, B., et al., 2013. *In vivo* random mutagenesis of streptomycetes using mariner-based transposon *Himar1*. Appl. Microbiol. Biotechnol. 97**,** 351-9.

Brown, S., et al., 2015. *De novo* production of the plant-derived alkaloid strictosidine in yeast. Proc Natl Acad Sci USA. 112**,** 3205-10.

Chater, K. F., Wilde, L. C., 1980. Streptomyces-Albus-G Mutants Defective in the Salgi Restriction-Modification System. Journal of General Microbiology. 116**,** 323-334.

Cuthbertson, L., Nodwell, J. R., 2013. The TetR family of regulators. Microbiol Mol Biol Rev. 77**,** 440-75.

De Paepe, B., et al., 2017. Tailor-made transcriptional biosensors for optimizing microbial cell factories. J. Ind. Microbiol. Biotechnol. 44**,** 623-645.

Dietrich, J. A., et al., 2010. High-throughput metabolic engineering: advances in small-molecule screening and selection. Annu Rev Biochem. 79**,** 563-590.

Dietrich, J. A., et al., 2013. Transcription factor-based screens and synthetic selections for microbial small-molecule biosynthesis. ACS Synth. Biol. 2**,** 47-58.

Emsley, P., Cowtan, K., 2004. Coot: model-building tools for molecular graphics. Acta Crystallographica Section D-Biological Crystallography. 60**,** 2126-2132.

Fedoryshyn, M., et al., 2008. Marker removal from actinomycetes genome using Flp recombinase. Gene. 419**,** 43-47.

Flett, F., et al., 1997. High efficiency intergeneric conjugal transfer of plasmid DNA from Escherichia coli to methyl DNA-restricting streptomycetes. FEMS Microbiol Lett. 155**,** 223-9.

Herrmann, S., et al., 2012. Site-Specific Recombination Strategies for Engineering Actinomycete Genomes. Applied and Environmental Microbiology. 78**,** 1804-1812.

Isaacs, F. J., et al., 2011. Precise manipulation of chromosomes in vivo enables genome-wide codon replacement. Science. 333**,** 348-53.

Jensen, P. R., Hammer, K., 1998. The sequence of spacers between the consensus sequences modulates the strength of prokaryotic promoters. Appl Environ Microb. 64**,** 82-87.

Kabsch, W., 2010. Xds. Acta Crystallographica Section D-Biological Crystallography. 66**,** 125-132.

Kieser T., B. M. J., Buttner M.J., Charter K.F., Hopwood D., 2000. Practical *Streptomyces* Genetics. . John Innes Foundation, Norwich, United Kingdom.

Le, T. B. K., et al., 2011. Structures of the TetR-like Simocyclinone Efflux Pump Repressor, SimR, and the Mechanism of Ligand-Mediated Derepression. Journal of Molecular Biology. 408**,** 40-56.

Liu, H. T., Naismith, J. H., 2009. A simple and efficient expression and purification system using two newly constructed vectors. Protein Expression and Purification. 63**,** 102-111.

Long, F., et al., 2008. BALBES: a molecular-replacement pipeline. Acta Crystallographica Section D-Biological Crystallography. 64**,** 125-132.

Mannan, A. A., et al., 2017. Fundamental Design Principles for Transcription-Factor-Based Metabolite Biosensors. ACS Synth Biol. 6**,** 1851-1859.

Mccoy, A. J., et al., 2007. Phaser crystallographic software. Journal of Applied Crystallography. 40, 658-674.

Myronovskyi, M., et al., 2011. beta-Glucuronidase as a sensitive and versatile reporter in actinomycetes. Appl. Environ. Microbiol. 77, 5370-5383.

Newman, D. J., Cragg, G. M., 2016. Natural Products as Sources of New Drugs from 1981 to 2014. J. Nat. Prod. 79, 629-661.

Novick, A., Weiner, M., 1957. Enzyme induction as an all-or-none phenomenon. Proc Natl Acad Sci USA. 43, 553-566.

Ostash, I., et al., 2008. Coordination of export and glycosylation of landomycins in *Streptomyces cyanogenus* S136. FEMS Microbiol. Lett. 285, 195-202.

Paddon, C. J., et al., 2013. High-level semi-synthetic production of the potent antimalarial artemisinin. Nature. 496, 528-+.

Porter, J. N., et al., 1952. Achromycin - a New Antibiotic Having Trypanocidal Properties. Antibiotics and Chemotherapy. 2, 409-410.

Raman, S., et al., 2014. Evolution-guided optimization of biosynthetic pathways. Proc. Natl. Acad. Sci. USA. 111, 17803-8.

Rebets, Y., et al., 2015a. Insights into the pamamycin biosynthesis. Angew. Chem. Int. Ed. Engl. 54, 2280-4.

Rebets, Y., et al., 2015b. Insights into the pamamycin biosynthesis. Angew Chem Int Ed Engl. 54, 2280-4.

Rebets, Y., et al., 2017. Cloning and Expression of Metagenomic DNA in Streptomyces lividans and Subsequent Fermentation for Optimized Production. Methods Mol Biol. 1539, 99-144.

Reichheld, S. E., et al., 2009. The induction of folding cooperativity by ligand binding drives the allosteric response of tetracycline repressor. Proc Natl Acad Sci USA. 106**,** 22263-8.

Rogers, J. K., Church, G. M., 2016a. Genetically encoded sensors enable real-time observation of metabolite production. Proc. Natl. Acad. Sci. USA. 113**,** 2388-93.

Rogers, J. K., Church, G. M., 2016b. Multiplexed engineering in biology. Trends Biotechnol. 34**,** 198-206.

Rogers, J. K., et al., 2015. Synthetic biosensors for precise gene control and real-time monitoring of metabolites. Nucleic Acids Res. 43**,** 7648-60.

Rogers, J. K., et al., 2016. Biosensor-based engineering of biosynthetic pathways. Curr. Opin. Biotechnol. 42**,** 84-91.

Romero-Rodriguez, A., et al., 2015. An overview on transcriptional regulators in *Streptomyces*. Bba-Gene Regul Mech. 1849**,** 1017-1039.

Siegele, D. A., Hu, J. C., 1997. Gene expression from plasmids containing the araBAD promoter at subsaturating inducer concentrations represents mixed populations. Proc Natl Acad Sci USA. 94**,** 8168-8172.

Siegl, T., et al., 2013a. Design, construction and characterisation of a synthetic promoter library for fine-tuned gene expression in actinomycetes. Metabolic Engineering. 19**,** 98-106.

Siegl, T., et al., 2013b. Design, construction and characterisation of a synthetic promoter library for fine-tuned gene expression in actinomycetes. Metab Eng. 19**,** 98-106.

Studier, F. W., Moffatt, B. A., 1986. Use of Bacteriophage-T7 Rna-Polymerase to Direct Selective High-Level Expression of Cloned Genes. Journal of Molecular Biology. 189**,** 113-130.

Tahlan, K., et al., 2008. Ligand recognition by ActR, a TetR-like regulator of actinorhodin export. J. Mol. Biol. 383**,** 753-61.

Tang, S. Y., Cirino, P. C., 2011. Design and application of a mevalonate-responsive regulatory protein. Angew. Chem. Int. Ed. Engl. 50**,** 1084-6.

Wang, B. J., et al., 2015. Amplification of small molecule-inducible gene expression via tuning of intracellular receptor densities. Nucleic Acids Res. 43**,** 1955-1964.

Xiang, S. H., et al., 2009. Application of a double-reporter-guided mutant selection method to improve clavulanic acid production in *Streptomyces clavuligerus*. Metab. Eng. 11**,** 310-8.

Zhang, M. M., et al., 2017. CRISPR-Cas9 strategy for activation of silent *Streptomyces* biosynthetic gene clusters. Nat. Chem. Biol.

Fig. 1. Schematic representation of architecture and features of whole-cell metabolite-specific biosensor. (a) Principal modules of biosensor architecture. TF – transcription factor, LBD – ligand binding domain, DBD – DNA binding domain. (b) Key characteristics of the biosensor dose-response curve. Operating range is the range of concentrations that can be differentiated by the system; the dynamic range is the intensity of output signal that can be detected.

Fig. 2. Development and characterization of G0 and G1 pamamycin-specific biosensors. (a) The core structure of pamamycin and its derivatives. Pamamycin 607: R1,R2,R3,R4,R6=Me; R5,R=H. (b) Schematic outline of genetic organization of G0 pamamycin biosensor. Thin black arrows indicate the location of promoters. Triangles mark the locations of PamR2 operator repeats. Dashed arrows show PamR2-operator repeats interactions. (c) Operating range of G0 (ATG26-27P) and G1 biosensors in *S. albus* Δ*pseB4* and *S. alboniger* Δ0734. Error bars represent standard deviation from biological replicates. (d) Dynamic range of G0 (ATG26-27P) and G1 biosensors in *S. albus* Δ*pseB4* and *S. alboniger* Δ0734. (e) Generation of G1 pamamycin biosensors by combining synthetic promoters of different strengths, PamR2 operators and different signal output parts. (f) Production of total pamamycins by *S. alboniger* DSM-40043 and its derivatives obtained with the use of G0 (brown) and G1 (blue) biosensors. Error bars represent standard deviation from biological replicates.

Fig. 3. Structure of apo-PamR2 and pamamycin 607-bound PamR2. (a) Structure of the apo-PamR2 homodimer in cartoon representation along two orientations rotated by 90°. The two subunits are shown in cyan and dark blue. (b) Structure of the pamamycin 607-bound PamR2 homodimer in cartoon representation. The two subunits are shown in bright and dark green.

$2F_o$-F_c electron density for bound pamamycin 607 is shown in dark blue at 2σ. In contrast to apo-PamR2, in the ligand-bound form, helix α0 forms crystal contacts with a symmetry-related PamR2-homodimer. The domain-swapped helix (α0) from a symmetry-related molecule at its putative physiological position in the PamR2 dimer is shown in magenta and pink in the upper panel. (c) Overlay of the apo-PamR2 and the pamamycin 607-bound PamR2 homodimer shown in cylinder representation. Ligand binding induces major conformational changes; black arrows depict changes involving αArm1, α4 and α8. Pamamycin 607 binding increases the distance between the DBD by 4 Å and induces a rotation of the DBD by ~10.5° (measured using P67 Cα atom in α3). Helix α0 has been omitted for clarity. (d) Structure of pamamycin-binding pocket of PamR2 protein, with residues important for ligand specificity shown as sticks. The amino-acid residues from different monomers of PamR2 are shown in light and dark green, according to the colour scheme in panels b and c. $2F_o$-F_c electron density for bound pamamycin 607 is shown in dark blue at 1.5 σ. Carbon atoms at positions R1-R5 are shown as spheres and highlighted according to the colour scheme used in panels e and f. (e) Schematic view of the PamR2-pamamycin 607 interaction. Residues from the respective PamR2 subunits are shown in light and dark green. Interactions restricting and/or shaping the size of the R1-R5 binding pockets are emphasized in grey. Residues subjected to site-directed mutagenesis are highlighted in red. (f) Schematic description of the PamR2-pamamycin 607 interaction in the mutated PamR2 proteins. Four amino-acid residues were replaced with synonymous with the larger side chains decreasing the size of the binding pocket.

Fig. 4. Generation and characterization of G2 pamamycin biosensors. (a) β-glucuronidase activity of G1 and G2 biosensors in *S. albus* Δ*pseB4* strains in the presence of increasing concentrations of various pamamycin derivatives. (e) β-glucuronidase activity of G1 and G2 biosensors in *S. albus* Δ*pseB4* strains in the presence of increasing concentrations of an equimolar mixture of pamamycin derivatives. Concentrations shown refers to the total level of pamamycins. (f) β-glucuronidase activity of G1 and G2 biosensors in *S. albus* Δ*pseB4* strains in the presence of different concentrations of pamamycins crude extract. Error bars represent standard deviation from biological replicates.

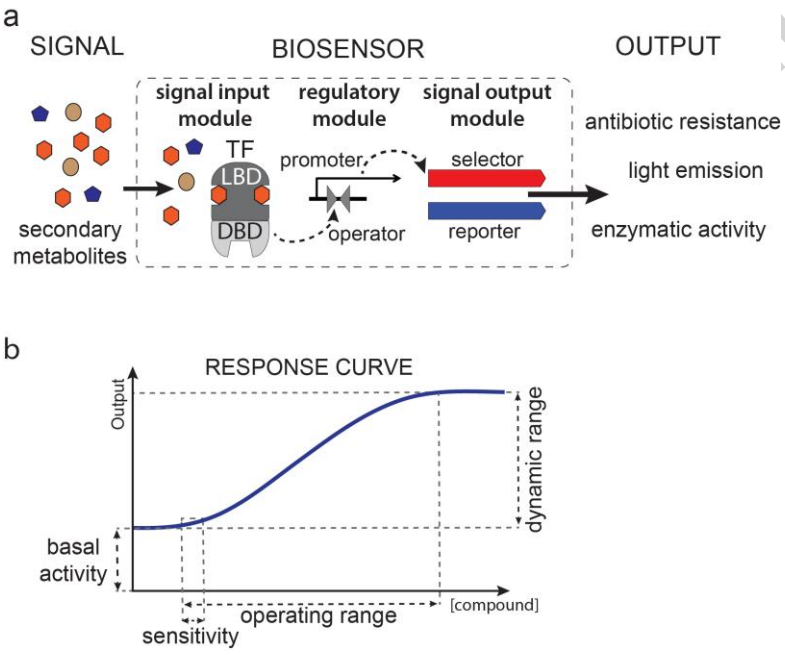

Figure 1. (single column)

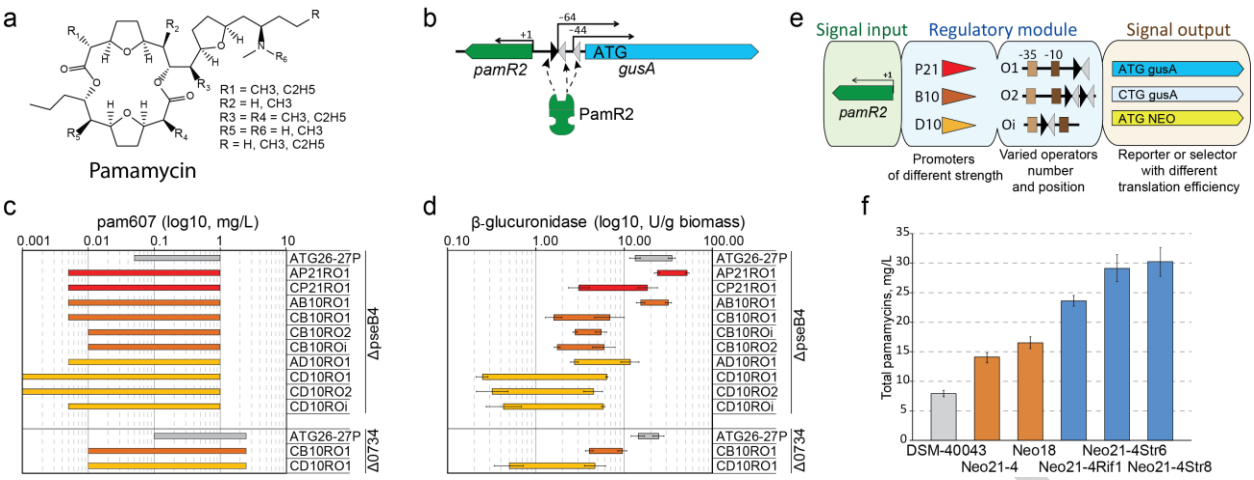

Figure 2. (2 columns).

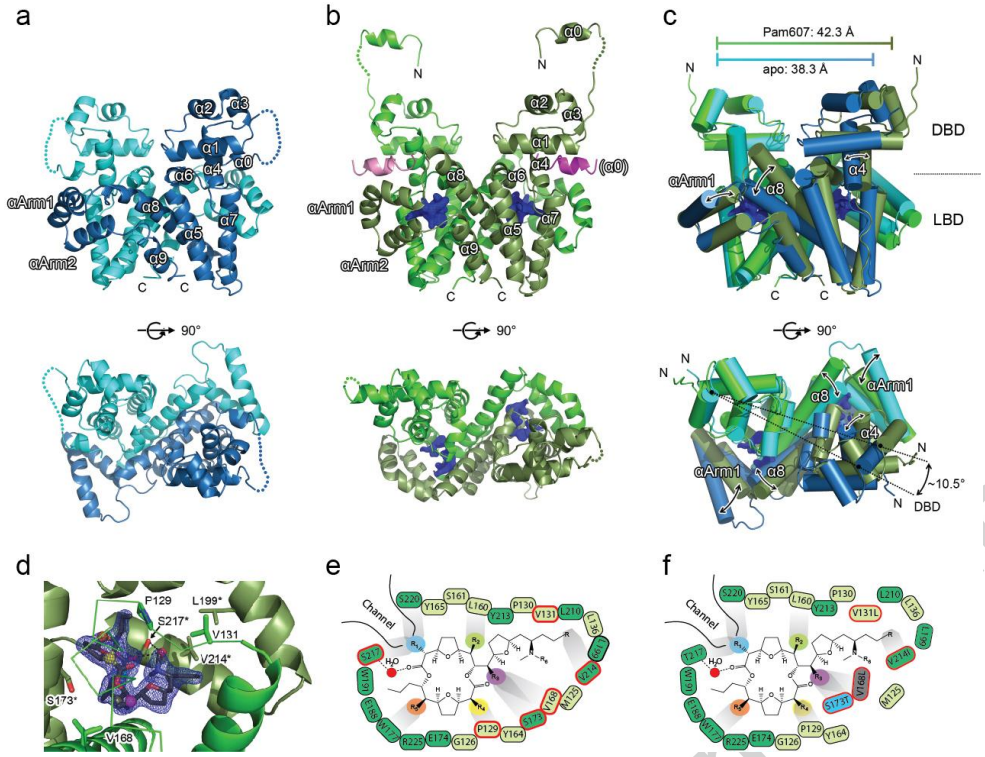

Figure 3. (1.5 column)

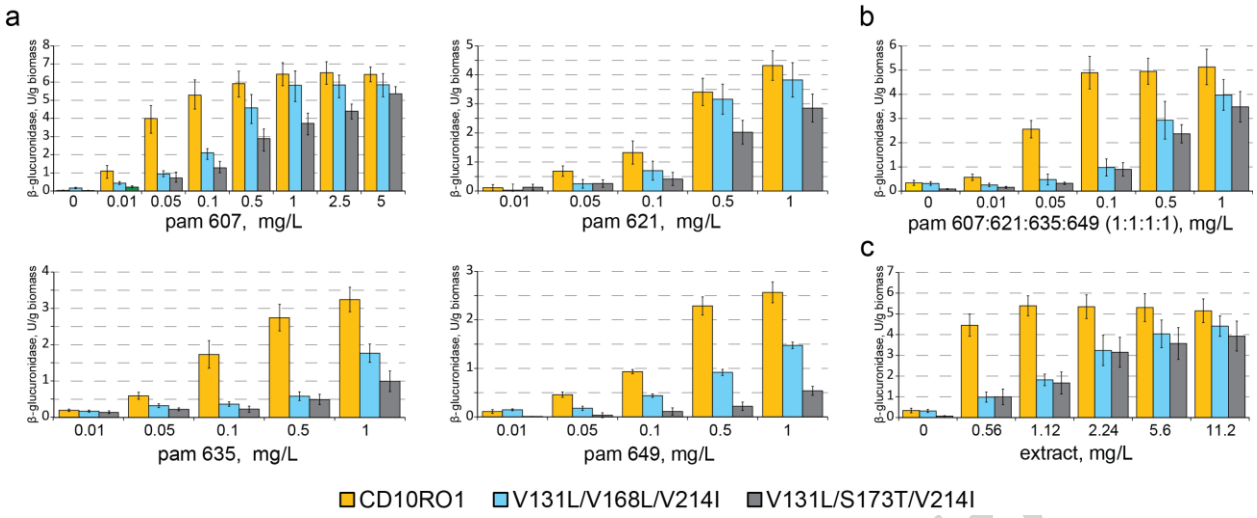

Figure 4. (2 columns).

Highlights

- The actinobacterial whole cell biosensor for antibiotic detection and quantification was constructed.
- The biosensor was applied in selection procedure to increase the yield of polyketide antibiotic pamamycin.
- The biosensor dynamic range was improved by tuning it's the signal output module.
- New biosensors with higher sensitivity were used in screening procedure for pamamycin overproducers and new producers.
- The biosensor performance was further improved by moderating ligand affinity of signal input module.